Manufacturing Technology and Research (An International Journal)| Volume 13 | Issue 1-2 | Jan-Dec(2020) ISSN: 0973-0281

An investigation into the Microstructural, Mechanical and Wear behaviour of the thin PVD coatings : A Comprehensive Review

Alok Vats[a], Dr. Amar Patnaik[b], Dr. M L Meena[c], Dr. Dinesh Shringi[d]

[a]Mechanical Engineering Department, MBM Engineering College, Jodhpur, India
alokvats1091@gmail.com
[b]Mechanical Engineering Department, MNIT Jaipur, India
apatnaik.mech@mnit.ac.in
[c]Mechanical Engineering Department, MNIT Jaipur, India
mlmeena.mech@mnit.ac.in
[d]Mechanical Engineering Department, MBM Engineering College, Jodhpur, India
drdshringi@gmail.com

Abstract

There are extreme wear surface phenomena such as abrasion, corrosion, erosion, oxidation etc. They create a number of performance and life issues in mechanical components whether stationary or in relative motion. Various surface treatment techniques are used in industrial practise to resolve these problems. Recently, coating techniques have been described as a cost-efficient way for surface alteration. Technique of Physical vapour deposition proves to be one of the most popular method among a wide range of available processes. The PVD system is generally recognised across industries because of its ability to provide wear and corrosion resistant coatings with characteristics such as superior thermal stability, hardness and better hardness to elastic modulus ratio (H/E ratio). PVD coatings can also be used in the development of thermal barrier coatings for high temperature applications. Deposition para-meters, like N_2 flow rate, base pressure, bias voltage, deposition temperature and deposition time, tend to have a major influence on coating properties. In this paper, a review of the mechanical aspects, wear behaviour, phase and chemical composition of the PVD coatings is done, in the light of the microstructure obtained. The review is relevant both from the industrial and research view-points.

Keywords: PVD; Microstructure; Tribological behavior; Mechanical.

1. Introduction

Physical Vapour Deposition (PVD) coating techniques are usually deployed by manufacturers and researchers to increase the component life. PVD is a one of the branch Vacuum coating technology. Other processes like Magnetron sputtering process also belong to the same class. These processes are used to deposit the hard materials over the substrate. These hard substances include both the oxide (TiO_x) coatings, the nitride (TiN, TiAlN) coatings as well as carbide (TiC) ones. They are grouped into three classes which include the CAE (Cathode Arc Evaporation), Magnetron sputtering and combined magnetron and arc sputtering. The difference between these coatings is the established on how the metallic or non- metallic target materials are converted from solid to vapour form. In the magnetron sputtering process, the Ar atoms are ionized using a strong magnetic field. They are bombarded on to the target. It causes the target atoms to be ejected towards the substrate material for deposition. This method is very energy efficient as compared to arc methods [1],[2]. While in the case of arc methods, the cathode area, which is very small, is provided with a high energy arc. The energy from this arc converts the solid target to vapour form. The schematic of PVD equipment has been shown in Fig. 1 while, PVD deposition process is shown in Fig. 2. Fig. 3 shows the schematic of CAE process set- up. Enhanced mechanical properties make PVD a better choice for industrial purposes. These properties include superior hardness, thermal stability and better hardness to elastic modulus ratio (H/E ratio). Due to the enhancement in the mechanical and wear behaviour, the PVD coatings are used in marine, high

temperature oxidation and excessive wear environments. As a result, the application areas of PVD coatings are many and quite diversified. They include Aircraft industry, Power plants, Automobile and Transportation sector, Hydraulic machinery, Petroleum, Printing and Paper industry, Manufacturing, Metal Processing and Textile Machinery etc. The reason for enhanced features of PVD coatings is their compact and hard microstructure with relatively less porosity. It is this microstructure which provides the PVD coatings its well-known coating characteristics. The microstructure of the PVD coatings depends on the deposition and geometrical parameters like pressure in vacuum chamber, Arc current, arc temperature, Nitrogen flow rate. The microstructure of PVD coatings may also contain the precipitates, hard phases and salts like nitrides, oxides and carbides. The conformance of these phases is done by XRD, EDAX, while the surface characterization is done by SEM analysis. In this paper a review on the influence of microstructure on the tribo-mechanical and wear behaviour of PVD coated layers, is done.

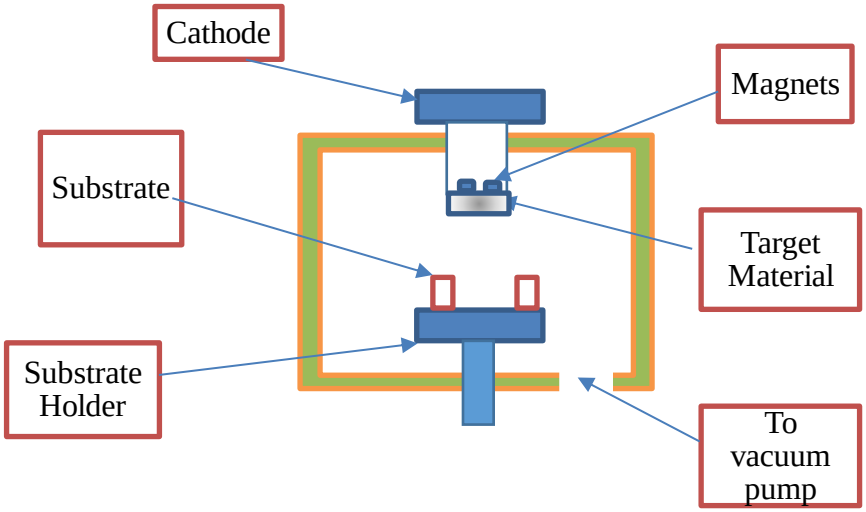

Fig. 1. Schematic PVD Coating process set up.

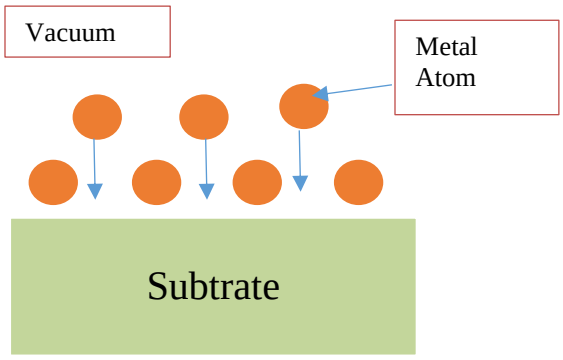

Fig. 2. The PVD deposition process.

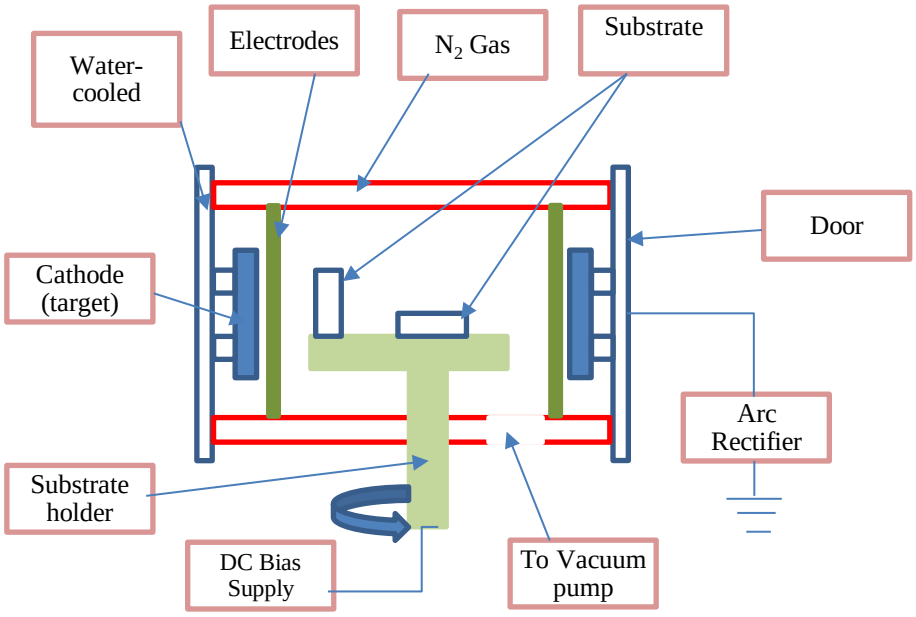

Fig. 3. Schematic of Cathode Arc Evaporation

2. Phase composition and microstructure

In a study, involving WC-Co-Cr powder, WC was the main phase and Co_3W_3C was the secondary phase. There was the formation of the solid solution of Co and Cr, as confirmed by the XRD peaks. Co_3W_3C was the product of decarburization of WC in the presence of Co and Cr [3]. Similar results were obtained in a study involving the cemented carbides in which the WC phase appeared bright and the Co binder phase appeared dark. The softness and ductility of Co binder, as well as the hardness & wear-resistance of WC particles provided a good combination to enhance overall performance. It improved the ability of the tools to sustain high-temperature effectively [4].

The spherical or flake α phase microstructure of Ti-6242S resulted in better fatigue strength, good thermal stability and fracture toughness. The duplex micro-structure of Ti-555 with few α phase b/w β phases provided it strength, plasticity and toughness. There was micro chipping for the first 5 minutes on (Ti-Al)N+Ti-N tools [5]. A columnar microstructure with high density and clear grain boundaries was observed while studying the behaviour of TiN coatings [6].

In a similar study, the CrN (thickness 1.80 µm) displayed a monolayer cubic microstructure. There was a primary deformation zone in near proximity of the interface b/w the chip and tool. Grain refinement was observed in this zone [7]. The uniform and dense microstructure of PVD coatings was obtained in AlTiN PVD 1 (2.5 µm monolayer) and PVD 2 (5 µm monolayer) [4]. In a study involving Ti-Nb alloy coating, the Nb was deposited by triode plasma Nitriding process. The coating had a dense columnar (cubic) structure with 33 atomic % Nb (Ti:Nb 2:1). The degree of coating crystallinity on Ti-AVM substrate was higher [8].

In a polymeric study, PTFE was found to consist of a long chain of C atoms. The F-atoms surrounded the C-atoms (ratio 1:2) and there existed a great bonding b/w them. PTFE thin film was deposited as the top layer. PTFE was present above the Al_2O_3 thin film [9]. The α-Zr phase (HCP crystal structure) was present in the Zr-4 alloy [10].

In another study, the attached droplets in TiAlN coatings, were loosely bonded to the coatings'

surface. The subsequent adhesion of WS_2 soft coatings suffered. The presence of micro-cracks at the WS_2/Ti-Al-N interface supported this phenomenon. These micro-cracks acted as nuclei, that resulted in fractures and cracks along the interface of WS_2/TiAlN coating system in early stages [11]. PVD technique could also be used to deposit materials like carbon (Avg. 26 μm thick) on the Ti-6Al-4V alloy system. In the XRD analysis of D-1250-1.6-70 sample, the peaks of TiN, TiO_2 and Ti_2AlC phase were found [12].

The XRD patterns of the ($Cr_{47}Al_{53}$) N coated samples had a cubic CrN and a cubic AlN phase. By adding Mo and Cu, there was a shift in the Cr-N and Al-N peaks at 2θ of 37.5° and 37.8°. The shift with Cu was less. And the formation of cubic Mo phases was favoured [13]. In another study, the bond and top coats were deposited during the coating process. They had different percentages of elements in them. The top coat had fairly large % of Zr, Y and O (small). While, the bond coat had large % of Ni, Cr, Al, O and C & Y (small). The presence of melted particles in the stationary substrate was more compared to the substrate rotating at 20 rpm [14]. The nitride coating like TiN grew on orientation plane (2 2 0) [15]. Crystalline phases like TiN (111) and TiO_2 (112) were found in the coatings deposited on Si (100) substrate at various angles [16].

The grain growth in the columnar microstructure decreased the hardness and mechanical strength of coatings. The multilayer state of the coatings prevented this [17]. Certain PVD coatings had the presence of nitride salt like TiN. In some of the PVD coatings a layered architecture was observed. It was seen that the modulation period decreased from 60 to 30 nm with the introduction of Ni[18].

The SEM was also used to study the interfacial area. This particular area exhibited either sharp (50 nm thick) or blurred (125 nm) images depending on coating thickness [19]. There was fine carbide particle formation, in the Co matrix in AlTiN (2.7 μm) and AlCrN (3.1 μm) coatings. The micro-defects were in the form of micro-holes, micro-droplets and macro defects. The oxide phase of CoO was evident as peaks at 2θ angles of 36.49°, 42.38°, 61.49° and 73.65 °respectively [20]. The features of PVD coatings like porosity and defects were exhibited in Fe_3Al coatings (120 μm thick). The presence of melted and un-melted particles was also observed. The CrN and DLC films (100 μm thick) were deposited on substrate [21].

3. Mechanical Aspects

3.1. Scratch test

Scratch test is usually conducted by means of a diamond stylus. In the case of softer coatings like WS_2, there was a low value of COF stabilization. After that, excessive plastic deformation increased the value of COF. Due to continued rubbing, the WS_2 layer was scraped off and TiAlN coating was exposed [11]. In the adhesion test of TiN coating (SS substrate), the first crack was at critical load of L_{c1} 13.6 N. The coating was up rooted at L_{c2} 17.2 N [6].

The maximum adhesive strength was observed at L_c = 14.1 N for coating no. 6. It was followed by detachment of the coating from substrate. A cohesive failure was observed in coating no. 8 at a critical load of 2.5 N. In this case, there was no detachment [22].

In the scratch test of the CrC hard coating, on Cu alloy, a gradual wear process was indicated. The fine scratch pattern with no sharp abrasive scratches of the CrC coated surface was visible [23].

3.2. Co-efficient of friction

In a study, there was a drop in the COF of the T-T-T samples. The middle layer was exposed. Diffusion took place up to atomic level (2500 cycles). Plasma Nitriding greatly improvement the wear resistance of nano-structured TiN coating [24]. In the case of [9], the wear mechanisms of cold-sprayed (Higher friction) and the sputtered (PVD) samples surfaces were different. This variation in COF was because of the production of wear debris. It increased the wear rate. The increase in the applied load and consequently, the loss of energy owing to excessive deformation (plastic) caused an increase in COF [9].

The evolution of the COF with sliding time for the steel-steel and the steel-TiN system was studied. lubrication of Glycerol (4 N load; 1.16 GPa contact stress) was used during the test. For uncoated steel, COF was 0.19 for the S-S (steel) system and 0.04 for steel+TiN system. The wear rate of uncoated steel disk was 8.3×10^{-5} $mm^3N^{-1}m^{-1}$.In a steel+TiN system, COF had a high value only during initial sliding. After 1000 s, it was gradually reduced to 0.018 [13]. For the C-C samples, after the run-in stage the average value of COF was in the range of 0.70–0.85. However, the COF increased to > 1.0 (4000 s), because of de-lamination of Ti-Al-N samples [11].

The COF was described as the function of sliding distance as in the case of untreated Ti-6Al-4V and D-1250-1.6-70 samples. A normal load of 10 N was applied. Average COF of the D- 1250-1.6-70 sample was reduced up to 66%, as compared to the Ti-6Al-4V sample [12].

The COF for coatings (Cr37Al50Mo13)N, (Cr5Al7Mo88)N and (Cr23Al31Mo40Cu6)N was in the range 0.08-0.1. For the (Cr34Al47Cu19)N coating, COF increased from 0.10 to 0.11, within the first 70 m. It was followed by a decline in the COF. After sliding distance of 300 m, the COF was around 0.10, indicating strong fluctuation in COF. Surface roughness also influences the COF. The variation of mean surface Roughness of the nitride coatings containing Mo and Cu is shown in Fig. 7 [13].

In the study of ion-bombarded TiN samples, the frictional force was quite unstable because of the wave-like pattern. In the scratch test, the TiN samples (low bombarding time) had higher adhesive properties, when compared to the high bombarding timed ones [15].

During the initiation of sliding, COF values were minimum but, they increased suddenly in the stage-II. The COF of Ti-6Al-4V substrate was 0.6 (unstable). The distance of sliding was 100 m and it caused excessive wear. The COF for C1 specimen was between $0.2 < \text{Friction}_{\text{co-efficient}} < 0.3$ before 50 m and became $0.3 < \text{Friction}_{\text{co-efficient}} < 0.4$ later on. Its average value was 0.38. The steady state was reached much earlier C2 and C3 [16]. In Al-Cr-N coatings, initially there was a peak in $\text{Friction}_{\text{co-efficient}}$. After that, the COF value was stabilised to 0.4 (after 0.05m of sliding). However, for Cr-W-N samples, the friction underwent peak initially and was stabilised to 0.45 [25]. There was a temperature function, involved in the COF of Al0.66Ti0.33N coating by arc PVD method. The graph between $\text{Friction}_{\text{co-efficient}}$ and coating distance was drawn in Ar jet environment. A COF of 0.2 was obtained at room temperature (10,000 cycles) [26].

There was a higher co-efficient of friction in un-reinforced PA (no G.F.). it was because of higher adhesion of PA to steel substrate. There was a reduced adhesion because of lesser polymeric contacts [27].

The schematic of the intrinsic factors (related to internal to coating features like formation of harder compounds inside coating during deposition and wear) influencing the COF of PVD coatings have been shown in Fig. 4. Also, the schematic of the extrinsic factors (related to external treatment on coating like EBH, LSP, presence of lubricating particles and compounds formed as a result of the pre and post treatments to coatings) influencing the COF of PVD coatings have been shown in Fig. 5.

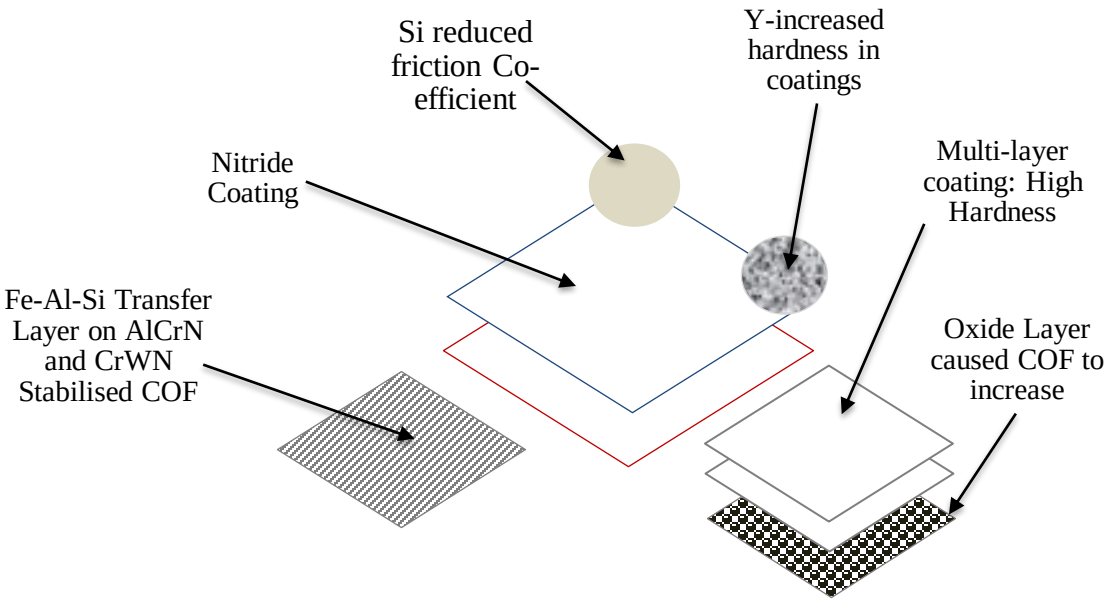

Fig. 4. Schematic of intrinsic factors influencing COF of PVD coating.

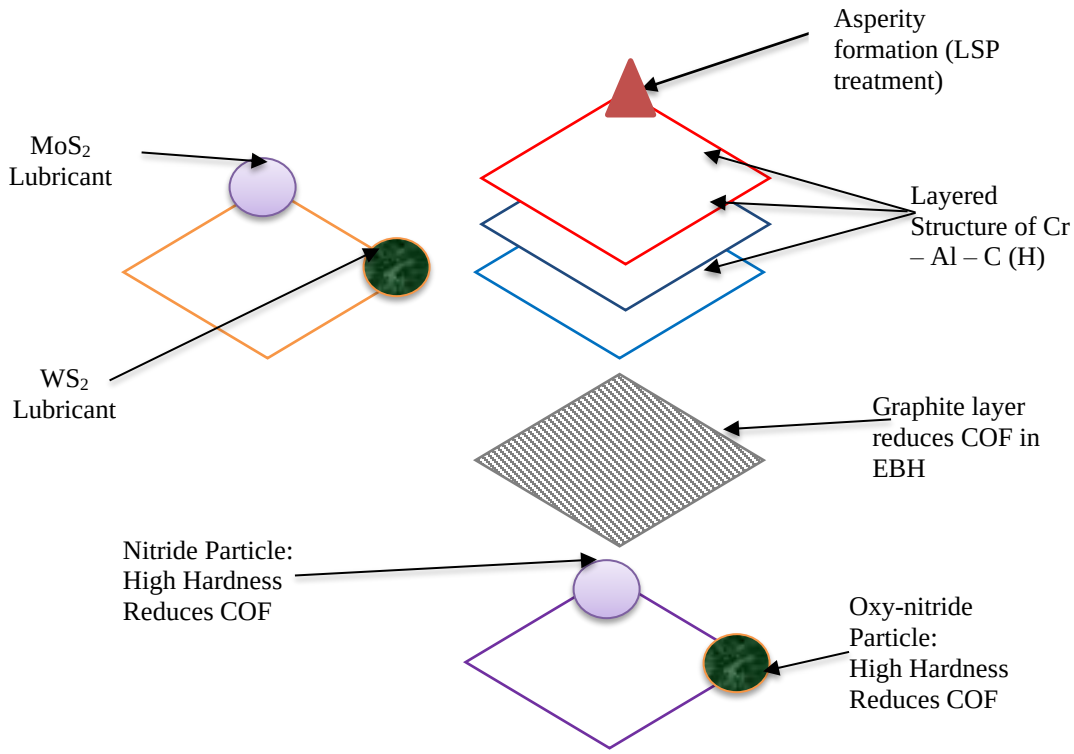

Fig. 5. Schematic of extrinsic factors influencing COF of PVD coating.

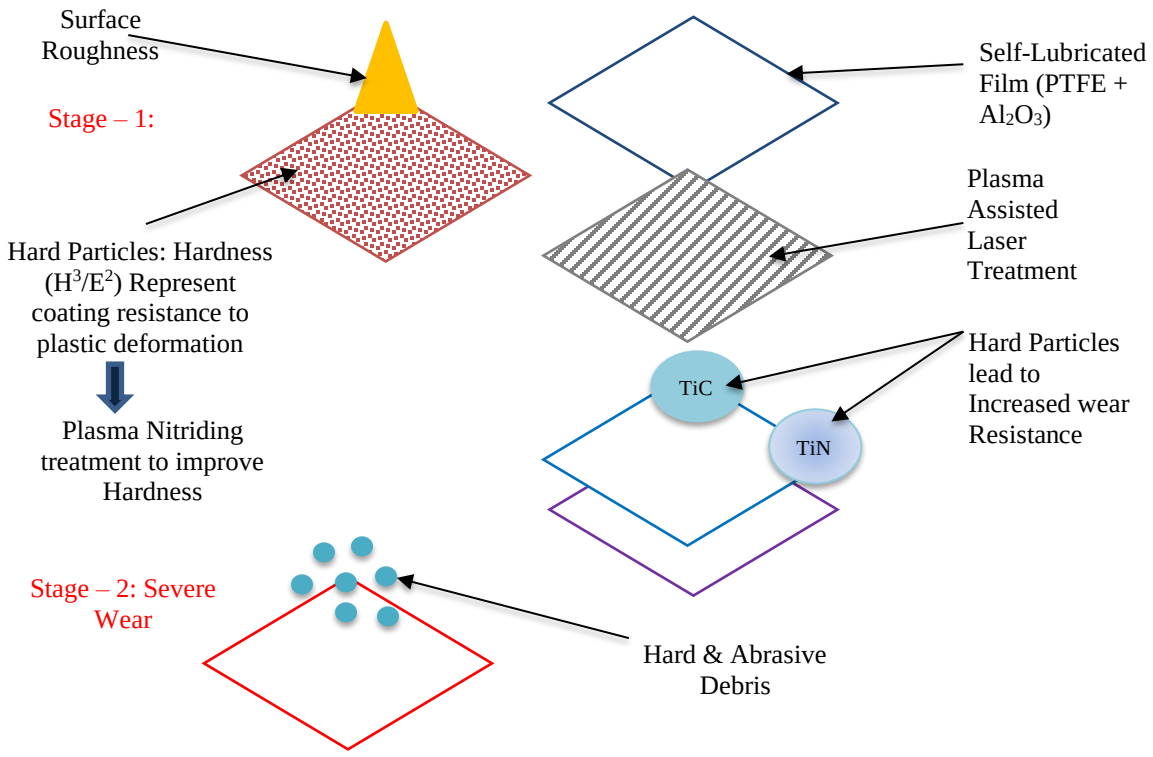

Fig. 6. Schematic of stages of friction behaviour of PVD coating.

The various stages of the friction behaviour of PVD coatings have been shown by the schematic diagram, as shown in Fig. 6.

In a study, the presence of Si in the CrN/AlCrN/ Al-Cr-Ti-Si-N hybrid coating with steel was responsible for the lowest friction co-efficient (μ=0.29), during the adhesion testing. It was followed by Cr/Cr-N (μ=0.32) & Cr/Cr-N/Al-Ti-Cr-N coatings (μ=0.48) [28].

In another study, there was formation of asperities, due to the Laser shock peening (LSP) treatments on the uncoated surface. It resulted in higher friction in contact with the sliding counter-part. Further increment in friction was due to the asperities getting rough and strain hardened. Higher friction led to greater heat generation at high speeds. There was an increase in adhesion due to this [28].

In a study, involving the DLC/Fe_3Al/SS- 304 and CrN-based duplex coatings, there was a decrease in the friction coefficient. It indicated that the environment (electrolytic) also had an influence over the COF. In case of, DLC-based coatings, there was an increase in the current after the wear tests for 200 s and 400 s. Initially, the DLC coatings were chemically inert. Continuous rubbing modified their chemical inertness. In case of CrN/Fe_3Al/ SS304-based coatings, there was a breakdown of thin protective film on the surface of the coating. Both rubbing and the film breakdown influenced COF values [21].

In the case of Mo-W-C coating, there was formation of compounds like MoS_2 and WS_2. They help in COF reduction. At high temperatures, the process of graphitisation became operational. It led to an increase in COF of DLC coatings [29].

The layered structure of Cr–Al–C (Cr_2AlC phase) helped in reducing COF as compared to Cr–Al–C(H) due to solid lubrication [30].

While studying the COF behaviour of the TiAlN/W_2N multi-layer coatings, there were two distinct phases, namely, the running state (RS-short nature) and the steady state (long). The RS was shorter in case of Ti-Al-N/W_2N multi-layer coatings as compared to stainless steel substrate. The COF of stainless steel substrate was nearly 0.86 in RS stage. For multi-layer coatings, it increased to 0.73–0.81 [39].

The friction behaviour is also influenced by method of PVD coatings and the gas flow rate. In a study involving W-C:H coatings by High Power Impulse Magnetron Sputtering method, the addition of H_2 reduced the RS stage and COF (from 0.14 to 0.06). In High Target Utilization Sputtering method, the addition of H_2 reduced the RS stage and COF (from 0.12 to 0.2) [40].

The COF values were lower for Electron Beam Hardening (EBH) treated coatings (μ as 0.2) as compared to the Electron Beam Re-melting (EBR) layers (μ as 0.6–0.8). This reduction in COF was due to lubrication by the graphite. It was also seen in the surface treatments like EBH+PVD and PVD+EBH [41].

In case of steel/TiN system, COF was 0.04 during sliding. It further decreased to 0.018 after sliding for a time period of 1000 s [6].

3.3. Composite &Multilayer PVD coatings

The TiAlN layers had FCC structure (NaCl type) with (220) plane orientation. So, Al substituted for Ti atoms in the TiN lattice and the solid solution of c-Ti(Al)N was formed. The peaks for Ti phase were detected in ML1 and ML2 coatings. The mass gain of SL1 coating increased steadily (80 cycles). After that, it began to increase rapidly. The mass gain of the other 3 coatings were consistently lower than that of SL1 coating during the cyclic oxidation process. The N_2 inward diffusion caused the formation of a compound layer composed of TiN and Ti_2N on the surface of the substrate, followed by an Al-rich layer and a N_2-stabilized Ti layer [34].

Excess of O_2 existed at the top surface of TiO_xN_y–TiN composite layered film due to the parent oxides. As the time for etching was increased, the N (atom level) conc. also increased, while O_2 concentration decreased. In the XRD patterns of CrN and TiO_xN_y–TiN sealed CrN (FCC structure) coatings, the CrN phase was present in planes of (111), (200) and (220). There was a red shift in the diffracted peaks for CrN, after the samples were sealed with ALD-TiN (360 °C) [35].

There was an interface formation b/w the inner layer of SiC and outer layer of ZrB_2-$MoSi_2$-SiC. Cracking did not take place. SiC nano-whiskers were present in the coating structure. The length of these nano-whiskers was less than 5 μm and their diameter was about 50–100 nm. ZrB_2 and $MoSi_2$ particles were also present. In the C/SiC/ZrB_2-$MoSi_2$-SiC samples, the two coats were there, namely, the top coat (ZrB_2-$MoSi_2$-SiC and 70 μm thick) and a bond coat (SiC overlay & 200 μm thick). White (secondary phase) particles were also present in the top coat of coating [36].

3.4. Surface Roughness

In a study, involving the Ti or Ti-Nb coatings, the Nitriding treatment led to an increase in the R_a values. Consequently, the PVD coatings deposited before the nitriding treatment had low R_a values. During the micro-abrasion testing, a greater R_a led to higher pressure of contact at the surface asperities. It fastened the detachment process of the (nitride) asperities. A reduced R_a value proved better for the Ti & Ti-Nb coating system in terms of the wear performance [8].

The substrate and the coating (29.0±2.0 μm) had a strong interface. Mechanical inter-locking enhanced the bonding between the two. The Cr layer for AR-Zr_4- Cr-PVD samples was 6.48±1.41 μm thick. The R_a value was 0.434 μm for the substrate AR-Zr_4 and 1.222 μm for the AR-Zr_4-Cr-

CS samples. The observed R_a of the coated samples was greater, as compared to the substrates. The structure and thickness of Cr coatings is shown in Fig. 8 [10].

There was a reduction in the peaks of blasted samples as compared to those of un-blasted ones. It was because of the abrasive action of media (MB) which levelled the droplets. There was an improvement in surface finish after micro-blasting process. Droplets' density at the top surface was also decreased. An optimal combination of micro-blasting and ion bombardment was necessary for enhanced wear resistance. It was observed that excessive micro-blasting alone was in-sufficient for better wear resistance [15].

The deposited films had very low R_a value. The R_a value of C_1 was higher in comparison to C_2 and C_3. There was an increase in the columnar size of TiO_2 layer (upper C_2 or C_3), as compared to TiN layer (upper C_1) [16].

Very low roughness values were found for LST+Al-TiN and LST+Al-CrN samples. The uniform growth of coating and a reduction in coating macro-particles' size were the reasons for low R_a of LST surfaces. As a result of it, the available surface area for coating was increased. The LSP samples had high R_a values for both coatings [20].

The indentation resistance of was for CrN (0.048 ± 0.006 μm) coatings in CrN/HSS samples. Initially there was now residual impression (10 Mn). The residual impressions dominated the scene, on increasing the force to 30 mN. Cracks in form of ring were formed at the force of 50 mN. There occurred cracking and removal of material b/w 30 to 50 mN. Such cracks depended on the energy of impact [37].

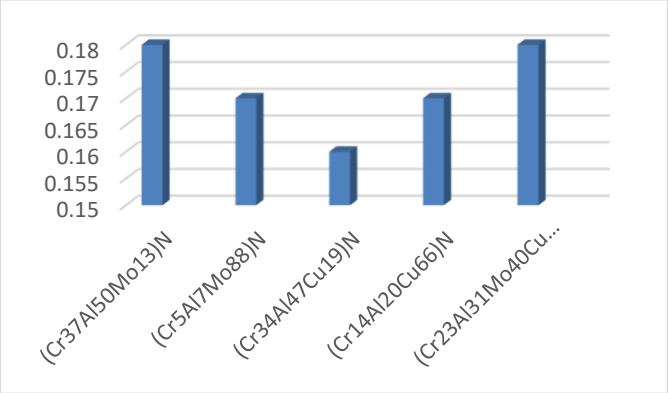

Fig. 7. Surface Roughness of the Mo and Cu containing nitride coating.

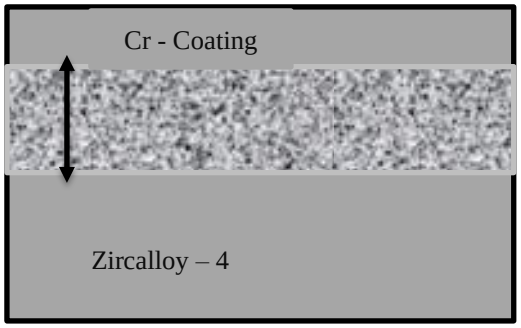

Fig. 8. Diagram depicting the structure and thickness of Cr coatings.

Despite the HVOF nature, there were pores and defects on the surface of the Fe_3Al (120 μm) coating due to the deposition process [21].

3.5. Hardness

The movement of the indenter with respect to coating thickness and the penetration depth influence the hardness level in case of Cr-coated samples. The AR-Zr4-Cr-PVD and AR-Zr4-Cr-CS layers were deposited on AR-Zr_4 substrate. 5 mN and 10 mN loads were employed for hardness measurement. The Cr-coatings were harder, as compared to that of the substrate [10]. The micro-hardness of the samples treated with laser was 2.5–4.5 times that of the substrate. The highest micro-hardness was in Ti-1.6-1250-D samples. The generation of hard and brittle compounds like TiC and TiN was the reason for this behaviour [12].

The influence of substrate movement (rotation) on hardness was also observed in certain coating types. The hardness of stationary substrate was 878.94 HV, while that of the rotating substrate was 834.66 HV [14]. In the multi-layer PVD coatings, it is the thickness of layers and their number which affects the micro-hardness. There is a direct relationship between the total coating thickness and hardness to be achieved [22]. However, there was a little influence of increase in coating thickness on mechanical properties like hardness, elastic modulus and mechanical strength [17]. The thicker alumina layer in TiAlN was α-Al_2O_3 modification. Also, the Y containing coatings of TiAlTaYN and TiAlYN showed similar hardness and Young's modulus values. Their hardness was greater than the samples without Y. Ta had no effect on any of the two properties [38]. Various treatment of the coating surfaces can also influence hardness. There was an increase in the hardness of the WC surface after LSP treatment. However, with the LST treatment, no change in hardness was observed for both un-coated and coated WC surfaces [20]. TiN (hardest coating) was studied in pre -(207 VHN) and post heat treatment (613 VHN) modes [39].

The addition of Ni (in nano-structured form) enhanced the level of hardness (37 to 45 GPa), young's modulus of Elasticity (601 to 662 GPa) and fracture toughness, as in case of Ti-Al-Mo-N PVD coatings. The increased values of H/E and H^3/E^2 parameters indicated the ductile nature of Ni containing coatings [18].

The difference in the structural aspects of the coatings also created a difference in hardness. In the case of Cr–Al–C (12.5 GPa) and Cr–Al–C(H) (8.9 GPa), the nano-inclusions (5–20 nm) of Cr_3C_2 and nano-crystalline graphite led to an increase in the hardness of Cr–Al–C [18].

Hardness also depended on the modulation period (MP) and number of layers in coatings. It was evident in the case of Ti-Al-N and W_2N coatings, where the multi-layer (ML) mode had higher hardness than the single layer mode. There was an increase in the hardness of TiAlN/W_2N ML (Max. hardness 1757 kgf·mm^{-2}) coatings up to a MP of 373 nm [31].

3.6. Coating thickness/ Porosity/ Stress

There was a little variation in thickness in the stationary substrate (207.59 mm thick) coatings, as compared to the rotating ones (200.40 mm thick). The speed of rotation was 20 rpm. Lesser number of pores were present in the surface of stationary substrate [14].

A residual state of stress existed for all coatings. However, the residual stress was low for T1-T3 coatings. The deposition parameters also influenced the state of stress. The SFC technology and a low bias voltage were the reasons for low residual stress. The increased thickness effected the tool geometry and mechanical properties of the coated inserts. Edge radius was increased as the coating became thicker [17].

4.Wear Performance

4.1. Tool wear

The coated tools show an enhanced wear resistance. The various factors that influence the wear were the feed, spindle speed, Friction property, cutting forces, cutting temperature and time for the test. Flank wear resistance was improved (43% reduction) by the TiAlN coated micro-drills [40].

Improper friction and large forces of cutting in uncoated tool, led to micro chipping. During milling of Ti-6242S (uncoated tool) the wear mechanisms were chipping, diffusion and adhesion. While, in case of Ti (C, N)+Al_2O_3+TiN coated tool micro-chipping and adhesion were main wear mechanisms. In (Ti, Al)N+TiN coated tool micro-chipping, diffusion and adhesion were (rake & flank face) predominant [5].

There was a reduction in the resultant forces in TiAlN-1 and TiAlN-2 coatings. The value of decrease was 27.46 and 23.51% for 90 m/min and 34.85 and 21.52% for120 m/min respectively. The cutting temperatures of TiAlN-1 and TiAlN-2 were also decreased, as compared with uncoated tool. During turning operation, the suitability of PVD Ti0.55Al0.45N coated tool was established for Inconel 718 at high cutting speeds of 90−120 m/min [41]. No detachment was seen in the CrN mono-layer PVD coating on $TiAl_6V_4$ alloy. the CrN coating had the ability to form thermal barrier films of Cr_2O_3. This influenced the intensity of crater wear strongly, leading to an increase in tool life [7]. Better plasticity and load carrying capacity rendered CVD 1 as the best performing coating. The tribological properties like CCR, metal flow and shear band were also enhanced. A combination of Co binder with TiC in CVD 1 reduced hardness and improved fracture toughness. There was not much effect of the thickness on the wear behaviour of PVD coatings [4].

The erosion wear amongst CrN, TiAlN and Ti-Al-N/CrN ($Ti_{45}Nb$ substrate) coatings, was maximum for CrN coating (8 $x10^{-3}$ mm^3/Nm). Also, the Erosion wear rate amongst Ti-Al-N (1), Al-Cr-N (2) and Ti-Al-Si-N (3) was maximum ($1.5x10^{-7}$ mm^3/Nm) for (1) and (2). The greatest hardness was for TiN coated AISI 304 because of the absence of Al. As the Si content was increased, the hardness also got improved (maximum value of 18.7 GPa at 5.09% Si) [24].

There was a change in the wear mechanism of Ti–6Al and Ti–10Al from adhesion to abrasion. The self-lubricating film (thin) was removed from the wear track completely. The primary wear mechanism for PVD sputtered Ti–6Al and Ti–10Al coated samples was abrasion. The inter-particle cracks were present on the worn surface. For cold-sprayed sub-surfaces, de-lamination and cohesion mechanisms dominated under high loads. The friction and wear were increased due to this [9].

The delamination dominated in PVD samples. No de-lamination was there in CS-coated Zr-4 alloy. The width and depth of the scratch was increased until the load reached critical length, L_c at 312 μm [10].

The ternary coatings like Ti-Al-N covered by WS_2 film (CC + W 6100 s; CM + W 7000 & 2850 s; CP + W 7800 & 4300 s; CF + W 7900 & 4400 s; CPF + W 8800 & 5200 s) exhibited a better wear resistance, as compared to the bare Ti-Al-N samples (CC 4000 s) [11].

On the samples (Cr37Al50Mo13)N – LVO – $100Cr_6$ (sample I), ($Cr_5Al_7Mo_{88}$)N – FVA_3+S – $100Cr_6$, ($Cr_{37}Al_{50}Mo_{13}$)N – FVA_3+S – Si_3N_4 and ($Cr_{23}Al_{31}Mo_{40}Cu_6$)N – FVA_3+S – Si_3N_4 slight wear tracks were detected. There was a strong co-relation b/w the increase in wear track's width (up to 6.60 X 10^{-2} microns), with the evolution of COF on sample I [13].

There was a direct relationship b/w the coefficient of wear and media pressure. The higher media pressure (upto 5 bar) and exposure time (upto 30 s) deteriorated the wear resistance property. Hence, optimal media pressure and time of exposure is desirable. A graph between the co-efficient of wear in Ti-N coating with time of exposure is plotted in Fig. 9 [15].

As the erodent particles were impinged on the coating, there started a reduction in the thickness

of coating. It occurred during the time of re-strained wear. Material loss was less in coating no. 8 as compared to the wear of coatings no. 1 and 2. The greatest stress (shear) τ_{max} existed at the edges of cleavages and micro-cracks. The lower the stress (shear) level, the better was the resistance of erosion. A graph of the erosion wear has been plotted in Fig. 10, depicting the above-said phenomena [22].

The stick and slip phenomena took place during the cutting process. The thicker, the coating, the better is the ability to withstand wear. It was also observed that T_2 coating underwent minimum wear [17].

In a particular study involving Cr / CrN layers, the cracks were formed. The generation of chips (both internal as well as external) was also observed at an increasing rate. Despite all these phenomena, the anti-wear properties of coatings were intact [28].

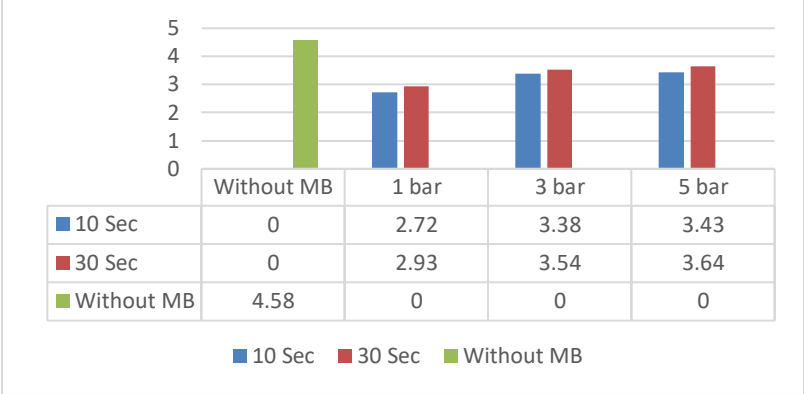

Fig. 9. Graph of the co-efficient of wear of Ti-N coating with time of exposure.

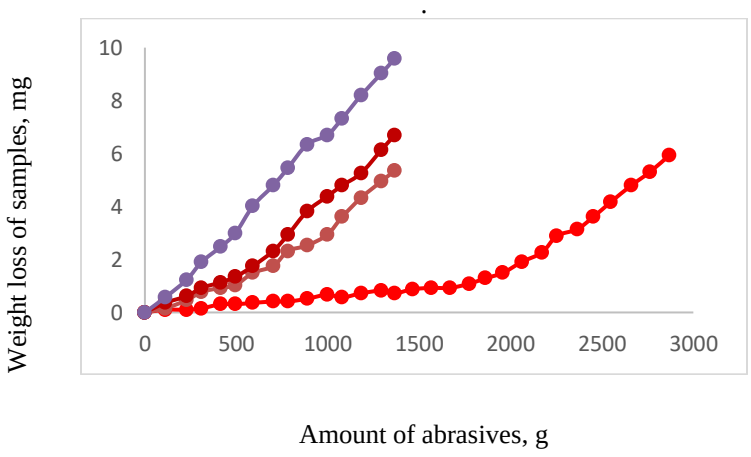

Fig. 10. Erosion wear of coatings.

4.2. Abrasion wear

The coating properties like hardness, fracture toughness and plasticity influenced the wear mechanism strongly. In a study, the Ti-Al-Mo-N coating had high fatigue resistance, good hardness and enough plasticity. As a result, the coatings suffered less wear and good resistance to the initiation and propagation of cracks. The mechanism of wear of Ti-Al-Mo-Ni-N and Ti-Al-

Mo-N coatings differed greatly at 500 °C [18].

There was a better exhibition of wear performance by TiAlTaYN samples, as compared to Ti-Al-Ta-N, Ti-Al-Y-N and Ti-Al-N counterparts. There were grooves located within the wear tracks, in all these coated samples. The wear track was wider for coating containing Y. The debris were mostly oxide particles [38].

The ternary coatings like Cr-W-N exhibited a higher wear resistance than the Al-Cr-N coating. Pressure of Contact was 5 MPa, sliding velocity 0.1 ms^{-1} and sliding distance 0.075m. Surface pores (less than micron size) generated lots of small wear debris. The 22Mn-B5 alloy steel deposited with Al-Si had brittle mechanical behaviour due to formation of the complex entities like Fe-Al-Si. There was a distinct interface between the Fe-Al layer of inter-metallic and PVD layers. This was mechanically attached and the homogenous in appearance suggesting that it was well bonded to the surface. There was large Al content in the inter-metallic complexes [25].

In a certain study, the coats were studied after a duration of 600 (Stage -1) and 1200 (stage – 2) cycles. In stage-1, Al-Cr-O coated tools had the lowest wear (0.4 $mm^{3)}$. It was followed by the DLC (0.8 mm^3). The other two coatings Ti0.57 Al0.43 N/Mo-Si-B and TiN/Mo-Si-B had greater material loss. In stage-2, the build-up volume increased for the DLC but reduced for the Al-Cr-O coating. The Ti0.57 Al0.43 N/Mo-Si-B multilayer coating also experienced a reduction in wear [19].

There were parallel grooves inside the wear track of the Fe_3Al/SS304 coating, as compared to the CrN/Fe_3Al/SS304 and the DLC/Fe_3Al/SS304 duplex coatings. Large pits were observed at this stage. A schematic showing wear tracks is shown in Fig.11[21].

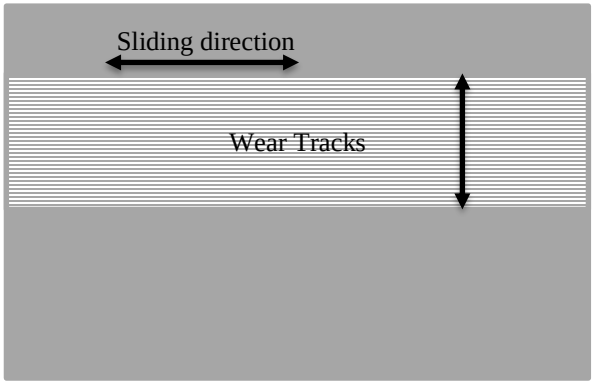

Fig. 11. Schematic of the surface of the wear track.

There was more wear in the areas where the carbide was exposed. The location of wear was in between WC grains. It covered partly the Co and consisted of both Cu and Zn. The transferred material on CrN coating was rich in the partly oxidized Zn [23].

The Salt Nitrided samples had a wear track of 4 μm. While, its value was less than 1 μm in the Ionic Nitrided samples. Nitriding experienced most of the wear in the initial discharge. It was followed by a less loss of material. The formation of Compound and Diffusion layers were responsible for such behaviour [27].

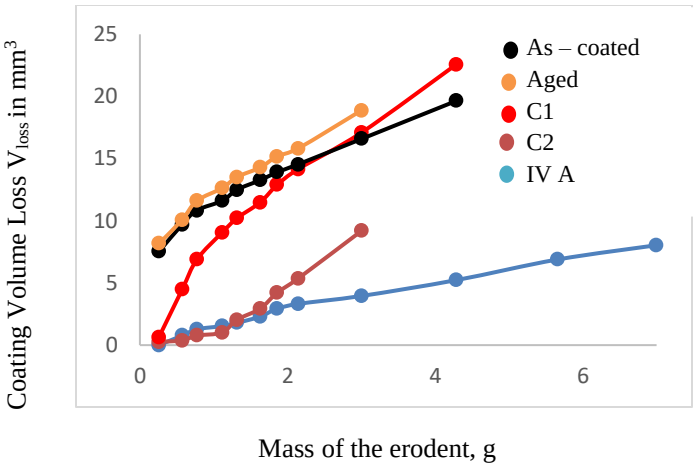

Fig. 12. Graph between Coating Volume Loss and Mass of erodent [42].

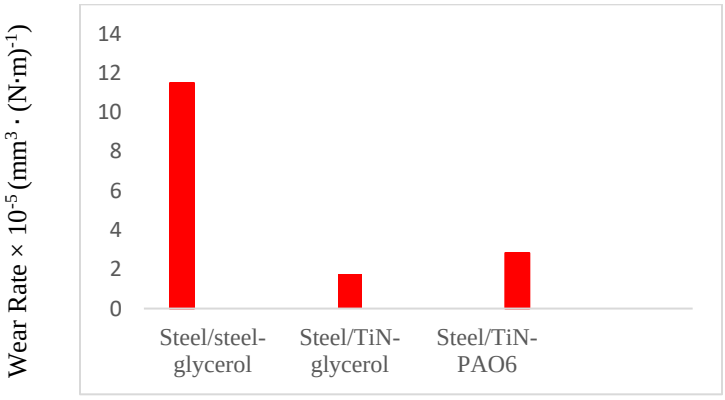

Fig. 13. Graph of wear rates for different specimen [6].

The wear rate of the uncoated steel disc was the highest (1.335×10^{-4} mm^3N^{-1} m^{-1}). It indicated that glycerol did not reduce the wear of steel effectively. The wear scars were in the form of scratches and furrows. The graph of the wear rates corresponding to various contact pairs in glycerol has been shown in Fig. 13 [6].

There was spalling of coatings' fragments during the cracking test of Cr–Al–C (900 mN load). This load exceeded the load to initiate cracking [27].

There were three distinct regions in the erosion wear of 7Y-S-Z coatings. Initially, there was erosion and spallation of Al_2O_3 layer. It was followed by a mixed erosion mode along with Al_2O_3 spallation. At this stage, erosion of 7-YSZ was initiated. Finally, erosion of 7-YSZ by delamination mode took place. The large erosion spot has been indicated as C1 (red) depicting the spallation of the alumina coating. The small erosion spot has been indicated as C2 (purple) & IVA (blue) depicting the progressive removal. After that a constant coating volume loss per erosion took place. The same phenomena has been shown on graph drawn in Fig. 12 [42].

References

[1] M. Ali (December, 2005). Review of physical vapour deposition (PVD) techniques hard coating.
[2] Physical Vapor Deposition (PVD) technology.
[3] B. Song, J. W. Murray, R. G. Wellman, Z. Pala and T. Hussain (2020). Dry sliding wear behaviour of HVOF

thermal sprayed WC-Co-Cr and WC-CrxCy-Ni coatings. *Wear*, vol. 442–443, pp. 1–10, 2020, doi: https://doi.org/10.1016/j.wear.2019.203114.

[4] Q. He, J. M. Paiva, J. Kohlscheen, B. D. Beake and S. C. Veldhuis (2020). An integrative approach to coating/carbide substrate design of CVD and PVD coated cutting tools during the machining of austenitic stainless steel. *Ceram. Int.*, vol. 46, no. 4, pp. 5149–5158, doi: 10.1016/j.ceramint.2019.10.259.

[5] M. C. Qinglong An, Jie Chen, Zhengrui Tao, Weiwei Ming (2019). Experimental investigation on tool wear characteristics of PVD and CVD coatings during face milling of Ti-6242S and Ti-555 titanium alloys. *Comp. Biochem. Physiol. Part C*, p. 108653, doi: 10.1016/j.cbpc.2019.108653.

[6] X. Fu, L. Cao, C. Qi, Y. Wan, and C. Xu (June 2020). Ultralow friction of PVD TiN coating in the presence of glycerol as a green lubricant.

[7] M. S. I. Chowdhury *et al.* (August 2019, 2020). Wear performance investigation of PVD coated and uncoated carbide tools during high-speed machining of TiAl6V4 aerospace alloy. *Wear*, vol. 446–447, no., doi: 10.1016/j.wear.2019.203168.

[8] G. Yumusak, A. Leyland, and A. Matthews (October 2019, 2020) . The effect of pre-deposited titanium-based PVD metallic thin films on the nitrogen diffusion efficiency and wear behaviour of nitrided Ti alloys. *Surf. Coatings Technol.*, vol. 394, doi: 10.1016/j.surfcoat.2020.125545.

[9] C. Ng, J. Rao and J. Nicholls (2019). The role of PVD sputtered PTFE and Al_2O_3 thin films in the development of damage tolerant coating systems. no. x x, pp. 1–12.

[10] R. V Umretiya, B. Elward, D. Lee, M. Anderson, R. B. Rebak and J. V Rojas (2020). Mechanical and Chemical Properties of PVD and Cold Spray Cr-coatings on Zircaloy-4.

[11] K. Zhang, X. Guo, C. Wang, F. Liu and L. Sun (2020). Effect of plasma-assisted laser pretreatment of hard coatings surface on the physical and chemical bonding between PVD soft and hard coatings and its resulting properties. Vol. 509, no. 8.

[12] M. Bahiraei, Y. Mazaheri, M. Sheikhi and A. Heidarpour (December 2019, 2020). A new approach to synthesis Ti_2AlC MAX phase using PVD coating and postlaser treatment. Vol. 385, no.

[13] K. Bobzin, C. Kalscheuer, C. Technology and C. Kalscheuer (2019). Arc PVD (Cr,Al,Mo)N and (Cr,Al,Cu)N Coatings for Mobility Applications.

[14] N. R. Kadam, G. Karthikeyan and D. M. Kulkarni (2020). Effect of substrate rotation on the microstructure of 8YSZ thermal barrier coatings by EB-PVD. *Materials Today : Proceedings* no. xxxx, pp. 8–13.

[15] R. Mundotia *et al.* (2020). Effect of ion bombardment and micro-blasting on the wear resistance properties of hard tin coatings. *Materials Today : Proceedings* no. xxxx.

[16] R. Bahi, C. Nouveau, N. E. Beliardouh, C. E. Ramoul, S. Meddah, and O. Ghelloudj (2020). Surface & Coatings Technology Surface performances of Ti-6Al-4V substrates coated PVD multilayered films in biological environments. Vol. 385, no. January.

[17] M. Abdoos, K. Yamamoto, B. Bose, G. Fox-Rabinovich and S. Veldhuis (2019). Effect of coating thickness on the tool wear performance of low stress TiAlN PVD coating during turning of compacted graphite iron (CGI). *Wear*, vol. 422–423, no. January, pp. 128–136, doi: 10.1016/j.wear.2019.01.062.

[18] V. S. Sergevnin, I. V. Blinkov, A. O. Volkhonskii, D. S. Belov and A. V. Chernogor (2019). Structure formation of adaptive arc-PVD Ti-Al-Mo-N and Ti-Al-Mo-Ni-N coatings and their wear-resistance under various friction conditions. *Surf. Coatings Technol.*, vol. 376, no. September, pp. 38–43, doi: 10.1016/j.surfcoat.2018.09.068.

[19] E. Aschauer *et al.* (2019). Adhesive wear formation on PVD coated tools applied in hot forming of Al-Si coated steel sheets. *Wear*, vol. 430–431, no. March, pp. 309–316, doi: 10.1016/j.wear.2019.05.019.

[20] S. K. Mishra, S. Ghosh and S. Aravindan (2019). Physical characterization and wear behavior of laser processed and PVD coated WC/Co in dry sliding and dry turning processes. *Wear*, vol. 428–429, no. March, pp. 93–110, doi: 10.1016/j.wear.2019.03.008.

[21] F. Pougoum *et al.* (2019). Study of corrosion and tribocorrosion of Fe_3Al-based duplex PVD/HVOF coatings against alumina in NaCl solution. *Surf. Coatings Technol.*, vol. 357, pp. 774–783, doi: 10.1016/j.surfcoat.2018.10.060.

[22] PVD- 2018-Erosive wear behavior of Ti_Ti(V,Zr)N multilayered PVD coatings for Ti-6Al-4V alloy.

[23] J. Heinrichs, H. Mikado, A. Kawakami, U. Wiklund, S. Kawamura and S. Jacobson (2019). Wear mechanisms of WC-Co cemented carbide tools and PVD coated tools used for shearing Cu-alloy wire in zipper production. *Wear*, vol. 420–421, no. October 2018, pp. 96–107, doi: 10.1016/j.wear.2018.12.075.

[24] G. Gupta, R. K. Tyagi, S. K. Rajput, P. Saxena, A. Vashisth and S. Mehndiratta (2020). PVD based thin film deposition methods and characterization / property of different compositional coatings - A critical analysis. *Materials Today : Proceedings*. no. xxxx.

[25] S. Mozgovoy, L. Alik, J. Hardell and B. Prakash (2019). Material transfer during high temperature sliding of Al-Si coated 22MnB5 steel against PVD coatings with and without aluminium. *Wear*, vol. 426–427, no. September 2018, pp. 401–411, 2019, doi: 10.1016/j.wear.2018.12.042.

[26] G. C. Mondragón-rodríguez, Y. Chipatecua-godoy, N. Camacho and D. G. Espinosa-arbeláez (2019). Effect of thermal treatments in high purity Ar on the oxidation and tribological behavior of arc-PVD c-Al0.66Ti0.33N coatings," *Surf. Coat. Technol.*, vol. 362, no. January, pp. 44–56, [Online]. Available: https://doi.org/10.1016/j.surfcoat.2019.01.070.

[27] B. Zabala *et al.* (2019). Mechanism-based wear models for plastic injection moulds. *Wear*, vol. 440–441, no. October 2018, doi: 10.1016/j.wear.2019.203105.

[28] Z. Gronostajski, M. Kaszuba, P. Widomski, J. Smolik, J. Ziemba and M. Hawryluk (2019). Analysis of wear mechanisms of hot forging tools protected with hybrid layers performed by nitriding and PVD coatings deposition. *Wear*, vol. 420–421, no. January, pp. 269–280, doi: 10.1016/j.wear.2019.01.003.

[29] P. E. Hovsepian and A. P. Ehiasarian (2019). Six strategies to produce application tailored nanoscale multilayer structured PVD coatings by conventional and High Power Impulse Magnetron Sputtering (HIPIMS). *Thin Solid Films*, vol. 688, no. April, 2019, doi: 10.1016/j.tsf.2019.137409.

[30] A. P. Rubshtein, K. Gao, A. B. Vladimirov, S. A. Plotnikov, B. Zhang and J. Zhang (2019). Structure, wear and corrosion behaviours of Cr–Al–C and multilayer [Cr–Al–C/a-C]n coatings fabricated by physical vapour deposition and plasma-assisted chemical vapour deposition techniques. *Surf. Coatings Technol.*, vol. 377, no. August, doi: 10.1016/j.surfcoat.2019.124912.

[31] X. Xu, F. Su, and Z. Li (2019). Tribological properties of nanostructured TiAlN/W2N multilayer coating produced by PVD. *Wear*, vol. 430–431, no. April, pp. 67–75, doi: 10.1016/j.wear.2019.04.021.

[32] F. Lofaj, M. Kabátová, L. Kvetková, J. Dobrovodský, and V. Girman (2019). Hybrid PVD-PECVD W-C:H coatings prepared by different sputtering techniques: The comparison of deposition processes, composition and properties. *Surf. Coatings Technol.*, vol. 375, no. August, pp. 839–853, doi: 10.1016/j.surfcoat.2019.07.078.

[33] A. Buchwalder and R. Zenker (2019). Pre- and post-surface treatments using electron beam technology for load-related application of thermochemical and PVD hard coatings on soft substrate materials. *Surf. Coatings Technol.*, vol. 375, no. August, pp. 920–932, doi: 10.1016/j.surfcoat.2019.07.084.

[34] Y. Cheng (January 2020). Cyclic oxidation behaviour of Ti/TiAlN composite multilayer coatings deposited on titanium alloy.

[35] K. Yato, S. Doi, A. Ishihara, S. Mitsushima, N. Kamiya and K. Ota (2006). Improved corrosion protection of CrN hard coating on steel sealed with TiOxNy-TiN composite layers. *J. Hydrog. Energy Syst. Soc. Japan*, vol. 31, no. 1, pp. 58–65.

[36] A. Abdollahi, Z. Valefi, and N. Ehsani (December, 2019). Erosion mechanism of ternary-phase SiC/ZrB_2-$MoSi_2$-SiC ultra-high temperature multilayer coating under supersonic flame at 90° angle with speed of 1400 m/s (Mach 4).

[37] X. Shi *et al.* (December 2020). Dynamic fracture of CrN coating by highly-resolved nano-impact. *Surf. Coatings Technol.*, vol. 383, no. doi: 10.1016/j.surfcoat.2019.125288.

[38] R. Aninat *et al.* (2019). Addition of Ta and Y in a hard Ti-Al-N PVD coating: Individual and conjugated effect on the oxidation and wear properties. *Corros. Sci.*, vol. 156, no. December 2018, pp. 171–180, doi: 10.1016/j.corsci.2019.04.042.

[39] S. Motru, N. Hussain, Z. Ali Khan and Avinash. Tribological studies of high surface finish ceramic coatings for low friction and adhesive wear resistant applications. *Mater. Today Proc.*, vol. 27, no. xxxx, pp. 2208–2212, 2019, doi: 10.1016/j.matpr.2019.09.098.

[40] S. Azim, S. Gangopadhyay, S. S. Mahapatra, R. K. Mittal and R. K. Singh (2020). Role of PVD coating on wear and surface integrity during environment-friendly micro- drilling of Ni-based superalloy.

[41] J. Zhao and Z. Liu (2020). Influences of coating thickness on cutting temperature for dry hard turning Inconel 718 with PVD TiAlN coated carbide tools in initial tool wear stage. *J. Manuf. Process.*, vol. 56, no. June 2019, pp. 1155–1165, doi: 10.1016/j.jmapro.2020.06.010.

[42] F.-L. T. c Lars Steinberg, Christoph Mikulla, Ravisankar Naraparaju and C. Holger Großmann Uwe Schulz , Christoph Leyens (2019). Erosion resistance of CMAS infiltrated sacrificial suspension sprayed alumina top layer on EB-PVD 7YSZ coatings. *Proc. Int. Therm. Spray Conf.*, vol. 2019-May, no. July, pp. 79–85.